

Controlled exploration of chemical space by machine learning of coarse-grained representations

Christian Hoffmann, Roberto Menichetti, Kiran H. Kanekal, and Tristan Berau*
Max Planck Institute for Polymer Research, 55128 Mainz, Germany
(Dated: March 26, 2025)

The size of chemical compound space is too large to be probed exhaustively. This leads high-throughput protocols to drastically subsample and results in sparse and non-uniform datasets. Rather than arbitrarily selecting compounds, we systematically explore chemical space according to the target property of interest. We first perform importance sampling by introducing a Markov chain Monte Carlo scheme across compounds. We then train an ML model on the sampled data to expand the region of chemical space probed. Our boosting procedure enhances the number of compounds by a factor 2 to 10, enabled by the ML model’s coarse-grained representation, which both simplifies the structure-property relationship and reduces the size of chemical space. The ML model correctly recovers linear relationships between transfer free energies. These linear relationships correspond to features that are global to the dataset, marking the region of chemical space up to which predictions are reliable—a more robust alternative to the predictive variance. Bridging coarse-grained simulations with ML gives rise to an unprecedented database of drug-membrane insertion free energies for 1.3 million compounds.

I. INTRODUCTION

Computational high-throughput screening ever-increasingly allows the coverage of larger subsets of chemical space. Extracting a property of interest across many compounds helps infer structure-property relationships, of interest both for a better understanding of the physics and chemistry at hand, as well as for materials design [1–4]. Recent hardware and algorithmic developments have enabled a number of applications of high-throughput screening in hard condensed matter [5, 6], while comparatively slower development in soft matter [7, 8].

Soft-matter systems hinge on a delicate balance between enthalpic and entropic contributions, requiring proper computational methods to reproduce them faithfully. Physics-based methodologies, in particular molecular dynamics (MD), provide the means to systematically sample the conformational ensemble of complex systems. High-throughput screening using MD presumably involves one simulation per compound. This remains computationally prohibitive at an atomistic resolution.

As an alternative, we recently proposed the use of coarse-grained (CG) models to establish a high-throughput scheme. Coarse-grained models lump several atoms into one bead to decrease the number of degrees of freedom [9]. The computational benefit of a high-throughput coarse-grained (HTCG) framework is twofold: (*i*) faster sampling of conformational space; but most importantly (*ii*) a significant reduction in the size of chemical space, tied to the transferable nature of the CG model (i.e., a finite set of bead types). Effectively the reduction in chemical space due to coarse-graining still leads to a combinatorial explosion of chemical space, but

with a significantly smaller prefactor. This many-to-one mapping is empirically probed by coarse-graining large databases of small molecules—an effort made possible by automated force-field parametrization schemes [10]. Using the CG Martini force field [11], we recently reported the *exhaustive* characterization of CG compounds made of one and two beads, corresponding to small organic molecules between 30 and 160 Da. Running HTCG for 119 CG compounds enabled the predictions of drug-membrane thermodynamics [12] and permeability [13] for more than 500,000 small organic molecules.

Pushing further our exploration of chemical space, how do we further diversify the probed chemistry in a systematic manner? Scaling up to larger molecular weight using more CG beads will ultimately lead to a combinatorial explosion: there are already 1,470 linear trimers and 19,306 linear tetramers in Martini. Instead of an exhaustive enumeration, we propose to explore regions of chemical space that are of particular interest. Specifically, rather than following the chemistry, we navigate chemical space according to the *target property*.

Akin to importance sampling used extensively to characterize conformational space, we first introduce a Markov chain Monte Carlo (MC) procedure to sample chemical compound space. Our methodology consists of a sequence of compounds where trial alchemical transformations are accepted according to a Metropolis criterion (Fig. 1a). While the acceptance criterion for conformational sampling typically includes the energy of the system, compositional sampling (i.e., across chemical space) means averaging over the environment and thus calls for a free energy—here applied to a solute molecule inserted in a phospholipid bilayer (Fig. 1b). As such, MC moves will favor compounds that increase their stability within a condensed-phase environment—algorithmically akin to constant pH simulations [14].

To further boost the size of chemical space that is probed, we further predict a more extended subset of

* berau@mpip-mainz.mpg.de

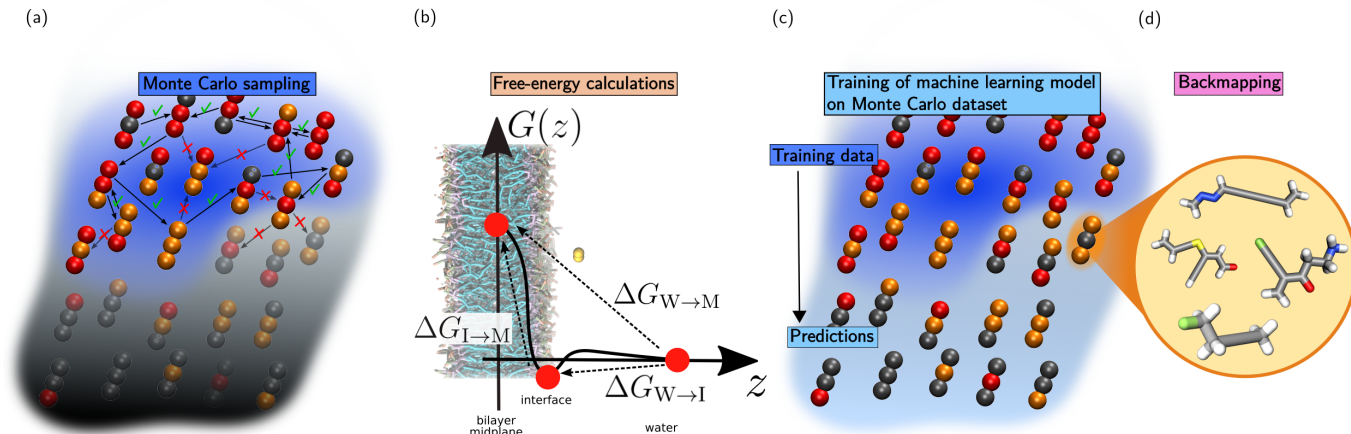


FIG. 1. (a) Importance sampling across coarse-grained compounds via a Markov chain Monte Carlo scheme. Only the dark-blue region is sampled. (b) Background: Simulation setup of a solute (yellow) partitioning between water (not shown) and the lipid membrane. Foreground: Potential of mean force along the normal of the bilayer, $G(z)$, and definition of the three transfer free energies of interest between the three state points (red circles): bilayer midplane (“M”), membrane-water interface (“I”), and bulk water (“W”). (c) The MC-sampled free energies (dark-blue region) form the training set for a machine learning model, used to predict a larger subset of compounds (light-blue region). (d) Each coarse-grained compound represents a large number of small molecules.

compounds that were not sampled by using machine learning (ML; see Fig. 1c) [15]. Despite known limited capabilities to extrapolate beyond the training set, we observe remarkable accuracy for the predicted compounds. This excellent transferability can be associated to a simplified learning procedure at the CG resolution: structure-property relationships are easier to establish [13] and compound similarity is compressed due to the reduction of chemical space. The range of reliable predictions is made clear by means of the ML model satisfying linear thermodynamic relations across compounds [12]—a more robust confidence metric compared to the predictive variance. The CG results are then systematically backmapped (Fig. 1d) to yield an unprecedentedly-large database of free energies.

II. RESULTS

We consider the insertion of a small molecule across a single-component phospholipid membrane made of 1,2-dioleoyl-*sn*-glycero-3-phosphocholine (DOPC) solvated in water. The insertion of a drug is monitored along the collective variable, z , normal distance to the bilayer midplane (Fig. 1b). We focus on three thermodynamic state points of the small molecule: the bilayer midplane (“M”), the membrane-water interface (“I”), and bulk water (“W”). We link these quantities in terms of transfer free energies, e.g., $\Delta G_{W \rightarrow M}$ denotes the transfer free energy of the small molecule from water to the bilayer midplane.

A. Importance sampling

We ran MC simulations across CG linear trimers and tetramers (results for tetramers are shown in the SI), randomly changing a bead type, calculating the relative free energy difference between old and new compound in the three different environments, and accepting the trial compound using a Metropolis criterion on the water/interface transfer free energy $\Delta G_{W \rightarrow I}$ (Fig. 1a). This criterion aimed at selecting compounds that favor partitioning in the membrane.

The MC algorithm yielded an acceptance ratio of 0.2. While initially most trial compounds contributed to expand the database, the sampling scheme quickly reached a stable regime where roughly half of the compounds had already been previously visited. Because each free-energy calculation is expensive, we avoid recalculating identical alchemical transformations to help efficiently converge the protocol.

A short MC sequence of accepted compounds is shown in Fig. S1. We display the sequence within the network of sampled compounds, each node being represented by the set of Martini bead types involved. Interestingly we find a large number of closed paths within this network. Since the free energy is a state function, the closed path represents a thermodynamic cycle—it must sum up to zero. We found negligible changes in the free energies regardless of whether or not this condition was enforced on the closed path, meaning that our chain of transformations does not compound significant statistical error.

B. Machine learning

We trained an ML model using the vector of water/octanol partitioning of each Martini bead type—one of their salient properties [10] (see Methods). When trained on most of the MC-sampled data, we obtained out-of-sample mean absolute errors (MAE) as low as 0.2 kcal/mol for $\Delta G_{W \rightarrow I}$ and $\Delta G_{I \rightarrow M}$, on par with the statistical error of the alchemical transformations (see Fig. S3). Remarkably, the prediction of $\Delta G_{W \rightarrow M}$ converges to an MAE lower than 0.05 kcal/mol, illustrative of the strong correlation between water/octanol and water/membrane free energies in Martini [12]. For all three quantities we monitor a correlation coefficient above 97%, indicating excellent performance.

Next, we train our ML model on the entire dataset of MC-sampled compounds. We use this model to predict all other CG linear trimers—a similar protocol was applied to tetramers. Because of the importance-sampling scheme, the predicted compounds will typically feature different characteristics, e.g., more polar compounds that would preferably stay in the aqueous phase. As such the ML model is technically extrapolating outside of the training set. As a measure of homogeneity between training and validation sets, Fig. 2 displays the distributions of confidence intervals (see Methods) between out-of-sample predictions and the expansion of the dataset. While we find significant overlap between the MC and ML distributions for trimers, we observe larger deviations in the case of tetramers.

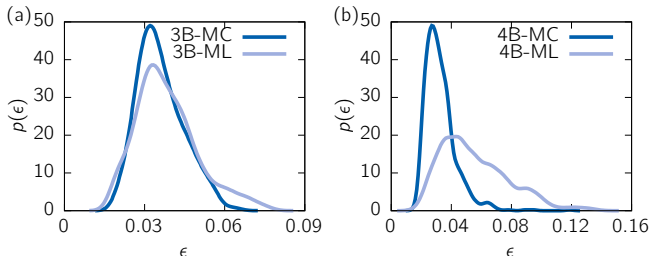


FIG. 2. Distribution functions of confidence intervals, $p(\epsilon)$ (see Methods for definition), for both the out-of-sample predictions within the MC-sampled compounds and the ML-predicted compounds. (a) Trimers and (b) tetramers.

The extrapolation can also be seen in the projections of predicted transfer free energies, highlighting distinct coverages of sampled and predicted trimer compounds (Fig. 3). Yet, the main panels (a) and (b) display notable linear relations between transfer free energies—similar behavior is found for tetramers (Fig. S4). Importantly, similar linear relations had already been observed for CG unimers and dimers, highlighting thermodynamic relations for the transfer between different effective bulk environments [12]. We also argue that the ML models do not simply learn linear features, since we optimize independent models for the different predicted transfer free

energies. They also offer higher accuracy compared to simple linear fits: mean-absolute error (MAE) of 0.3 and 0.5 kcal/mol for the ML and linear fit, respectively, across a small set of 50 reference compounds spanning the entire dataset. The linear behavior displayed across both sampled and predicted compounds testifies to the robustness of the ML model, despite the extrapolation.

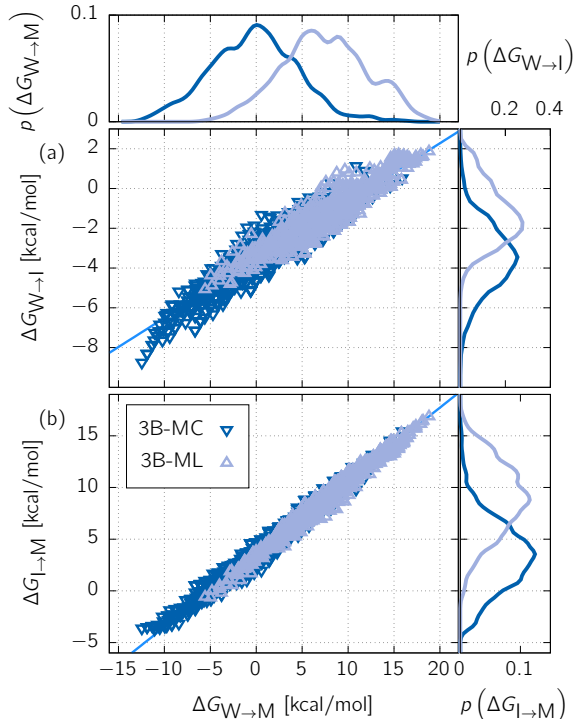


FIG. 3. (a) Transfer free energies from water to interface $\Delta G_{W \rightarrow I}$ as a function of the compounds water/membrane partitioning free energy, $\Delta G_{W \rightarrow M}$. The dark and light blue points depict corresponding quantities for trimers estimated from MC sampling (3B-MC) and the ML predictions (3B-ML), respectively. Linear fits highlight the molecular-weight dependence. (b) Transfer free energies from the interface to the membrane $\Delta G_{I \rightarrow M}$ as a function of the compound’s water/membrane partitioning free energy, $\Delta G_{W \rightarrow M}$. The coverages are projected down along a single variable on the sides. Error bars for 3B-MC are on par with the datapoint sizes (not shown).

A systematic coarse-graining of compounds in the GDB [16] using AUTO-MARTINI [10] was performed to identify small organic molecules that map to CG linear trimers. We identified 1.36 million compounds, for which we can associate all three transfer free energies, $\Delta G_{W \rightarrow M}$, $\Delta G_{W \rightarrow I}$, and $\Delta G_{I \rightarrow M}$. We note that the sampled and predicted CG representations amount to similar numbers of compounds, such that the ML boosting introduced here offers an additional 0.8 million compounds to the database. The database is provided as supporting material for further data analysis.

III. DISCUSSION

The overwhelming size of chemical space naturally calls for statistical techniques to analyze it. A variety of data-driven methods such as quantitative structure-property relationships (QSPR) and ML models at large have been applied to chemical space [17–20]. While sparse databases easily lead to overfitting [21], a dense coverage can offer unprecedented insight [22]. Here we rely on tools from statistical physics to ease the exploration of chemical space: the application of importance sampling guides us toward the subset of molecules that enhance a desired thermodynamic property. The latter is akin to recent generative ML models [23], but without the *a priori* requirement for labeled training data.

A conceptually-appealing strategy to expand the MC-sampled distribution is through an ML model. Effectively we train an ML model on the MC samples and further boost the database with additional ML predictions. Unfortunately, the limited extrapolation behavior of kernel models means that accurate predictions can only be made for compounds *similar* to the training set. *How* similar is often difficult to estimate *a priori*. Similarity metrics are often based at the level of the ML’s input space—here the molecular representation. In Fig. 2 we used the predictive variance as a metric for the query sample’s distance to the training set [15].

Beyond similarity in the ML’s input space via the predictive variance, we also consider the target properties directly. Our physical understanding of the problem offers a clear requirement on the transfer free energies, through the linear relationships shown in Fig. 3 [12]. As such, the thermodynamics of the system impose a physically-motivated constraint on the predictions. Rather than specific to each prediction, this constraint is *global* to the ensemble of data points. Satisfying it grounds our predictions within the physics of the problem, ensuring that we accurately expand the database.

Remarkably, we find that we can significantly expand our database—doubling it for trimers and a factor of 10 for tetramers (see SI)—while retaining accurate transfer free energies. Unlike conventional atomistic representations [24], our ML model is encoded using a CG representation, such that compounds need only be similar at the CG level. This CG similarity is strongly compressed because (i) coarse-graining reduces the size of chemical space [12], but also (ii) of a more straightforward structure-property link [13]. The latter is embodied by the additive contribution of bulk partitioning free energies for each bead, efficiently learning the molecular transfer free energy in more complex environments. All in all, backmapping (Fig. 1d) significantly amplifies the additional region of chemical space reached by the ML model. Our work highlights appealing aspects of bridging physics-based methodologies and coarse-grained modeling together with machine learning, offering better robustness and transferability to explore significantly broader regions of chemical space.

IV. METHODS

A. Coarse-grained simulations

MD simulations of the Martini force field [11] were performed in GROMACS 5.1. The integration time-step was $\delta t = 0.02 \tau$, where τ is the model’s natural unit of time. Control over the system temperature and pressure ($T = 300 \text{ K}$ and $P = 1 \text{ bar}$) was obtained by means of a velocity rescaling thermostat [25] and a Parrinello-Rahman barostat [26], with coupling constants $\tau_T = \tau$ and $\tau_P = 12 \tau$. Bulk simulations consisted of $N_W = 450$ and $N_O = 336$ water and octane molecules, where the latter was employed as a proxy for the hydrophobic core of the bilayer [12]. As for interfacial simulations, a membrane of 36 nm^2 containing $N_L = 128$ DOPC lipids (64 per layer) and $N'_W = 1890$ water molecules was generated by means of the INSANE building tool [27], and subsequently minimized, heated up, and equilibrated. In all simulations containing water molecules we added an additional 10% of antifreeze particles.

B. Free-energy calculations

Water/interface and interface/membrane transfer free energies $\Delta G_{W \rightarrow I}$ and $\Delta G_{I \rightarrow M}$ for all compounds investigated in this work were obtained from alchemical transformations, in analogy with Ref. [12]. This construction is based on the relation linking the transfer free energies of two compounds A and B ($\Delta G_{W \rightarrow I}^A$, $\Delta G_{W \rightarrow I}^B$ and $\Delta G_{I \rightarrow M}^A$, $\Delta G_{I \rightarrow M}^B$) to the free energies of alchemically transforming A into B in the three fixed environments, $\Delta G_I^{A \rightarrow B}$, $\Delta G_W^{A \rightarrow B}$ and $\Delta G_M^{A \rightarrow B}$

$$\Delta G_{W \rightarrow I}^B = \Delta G_{W \rightarrow I}^A + (\Delta G_I^{A \rightarrow B} - \Delta G_W^{A \rightarrow B}),$$

$$\Delta G_{I \rightarrow M}^B = \Delta G_{I \rightarrow M}^A + (\Delta G_M^{A \rightarrow B} - \Delta G_I^{A \rightarrow B}). \quad (1)$$

$\Delta G_I^{A \rightarrow B}$, $\Delta G_W^{A \rightarrow B}$, and $\Delta G_M^{A \rightarrow B}$ were determined by means of separate MD simulations at the interface, in bulk water, and in bulk octane. For the calculation of each $\Delta G_i^{A \rightarrow B}$, $i = I, W, M$ we relied on the multistate Bennett acceptance ratio (MBAR) [28, 29], in which free-energy differences are obtained by combining together the results from simulations that sample the statistical ensemble of a set of interpolating Hamiltonians $H(\lambda)$, $\lambda \in [0, 1]$, with $H(0) = H_A$ and $H(1) = H_B$. We employed 24 evenly spaced λ -values for each alchemical transformation and in each environment (interface, water, octane). The production time for each λ point was $4 \cdot 10^4 \tau$ at the interface and $2 \cdot 10^4 \tau$ in bulk environments. To calculate $\Delta G_i^{A \rightarrow B}$ we added a harmonic potential with $k = 1000 \text{ kJ mol}^{-1} \text{ nm}^{-2}$ between the compound and the bilayer midplane at a distance $z = 1.5 \text{ nm}$ to account for the spatial localization of the interface.

C. Monte Carlo sampling

We perform a stochastic exploration of the chemical space of CG linear trimers and tetramers through the generation of Markovian sequences of compounds. Given the last compound A of a sequence, the new compound B is proposed by randomly selecting a bead of A and changing its type. The move from A to B is then accepted with probability

$$P_{A \rightarrow B} = \min \left\{ 1, \exp \left[-\beta (\Delta G_{W \rightarrow I}^B - \Delta G_{W \rightarrow I}^A) \right] \right\}, \quad (2)$$

where $\Delta G_{W \rightarrow I}^A$ and $\Delta G_{W \rightarrow I}^B$ are the water/interface transfer free energies of A and B , respectively. This choice for $P_{A \rightarrow B}$ aims at driving the Monte Carlo sampling towards compounds that favor partitioning in the membrane. While in this work we set $\beta = 1/k_B T$, we stress that β can in principle be chosen independently of the system temperature. The free-energy difference in Eq. 2 is derived from the alchemical free-energy differences of transforming A into B in the three fixed environments $\Delta G_i^{A \rightarrow B}$, $i = W, I, M$ (first relation in Eq. 1), which we compute from MD simulations.

We generated up to five independent Markovian sequences in parallel, each starting from a different initial compound. To avoid recalculating alchemical transformations already visited, we stored the history of calculations and looked up previously-calculated values when available.

D. Thermodynamic-cycle optimization

We reconstructed the transfer free energies $\Delta G_{W \rightarrow I}$ and $\Delta G_{I \rightarrow M}$ for all compounds analyzed in this work as a summation over a sequence of alchemical transformations by means of Eq. 1 (Fig. S1). The outcome of our Monte Carlo sampling consists of an ‘‘alchemical network’’ in which each node of the network represents a compound, and an edge connecting two nodes A and B corresponds to an alchemical transformation that was sampled via an MD simulation, see Fig. S1. Each edge is characterized by the free-energy differences $\Delta G_i^{A \rightarrow B}$ in the three fixed environments, $i = W, I, M$.

For each environment, the net free-energy difference along any closed cycle in the network must be zero, by virtue of a free energy being a state function. We thus enforced this thermodynamic condition to optimize the set of free-energy differences calculated from MD simulations. We employed the algorithm proposed by Paton [30] to identify the cycle basis that spans the alchemical network, i.e., each cycle in the network can be obtained as a sum of the N_C basis cycles. We denote the MD free-energy differences involved in at least one basis cycle by ΔG_i^j , $j = 1, \dots, N_C$, $i = W, I, M$, while nodes connected to only a single edge cannot be taken into account. For each environment, we optimized the set of free energies

$\Delta \hat{G}_i^j$ by minimizing the loss function

$$\mathcal{L}_i = \sum_{j=1}^{N_C} (\Delta G_i^j - \Delta \hat{G}_i^j)^2 + \sum_{k=1}^{N_c} \omega \left(\sum_{j \in k} (-1)^{s_{j,k}} \Delta \hat{G}_i^j \right)^2. \quad (3)$$

While the first term ensures that the optimized free-energy differences $\Delta \hat{G}_i^j$ remain close to the MD simulation results, the second term ($\omega = 10.0$) penalizes deviations from zero for each thermodynamic cycle within a basis cycle. The exponent $s_{j,\alpha}$ controls the sign of the free-energy difference in the cycle, taking values of 0 or 1. To minimize the cost functions, we employed the Broyden-Fletcher-Goldfarb-Shanno method (BFGS) [31] (see Fig. S2).

E. Machine learning

We use kernel ridge regression [15], where the prediction of target property $p(\mathbf{x})$ for sample \mathbf{x} is expressed as a linear combination of kernel evaluations across the training points \mathbf{x}_i^* :

$$p(\mathbf{x}) = \sum_i \alpha_i K(\mathbf{x}_i^*, \mathbf{x}). \quad (4)$$

The kernel consists of a similarity measure between two samples

$$K(\mathbf{x}, \mathbf{x}') = \exp \left(-\frac{\|\mathbf{x} - \mathbf{x}'\|_1}{\sigma} \right), \quad (5)$$

which corresponds to a Laplace kernel with a city-block metric (i.e., L_1 -norm), and σ is a hyperparameter. The optimization of the weights α consists of solving for the samples in the training with an additional regularization term λ : $\alpha = (\mathbf{K} + \lambda \mathbf{I})^{-1} \mathbf{p}$. The confidence of the prediction is estimated using the predictive variance

$$\epsilon = \mathbf{K}^{**} - (\mathbf{K}^*)^T (\mathbf{K} + \lambda \mathbf{I})^{-1} \mathbf{K}^*, \quad (6)$$

where \mathbf{K}^{**} and \mathbf{K}^* represent the kernel matrix of training with training and training with test datasets, respectively [15]. The two hyperparameters σ and λ were optimized by a grid search, yielding $\sigma = 100$ and $\lambda = 10^{-4}$. Learning curves are shown in Fig. S3.

The representation ought to include enough information to distinguish a compound’s chemical composition and geometry, as well as encode the physics relevant to the target property [32]. Because the CG compounds all consist of beads arranged linearly and equidistant, we have found that encoding the geometry had no benefit to the learning (data not shown). Instead we simply encode the water/octanol partitioning of each bead, yielding for linear trimers $\mathbf{x} = \left(\Delta G_{W \rightarrow OI}^{(1)}, \Delta G_{W \rightarrow OI}^{(2)}, \Delta G_{W \rightarrow OI}^{(3)} \right)$. Note that while the problem we consider in this work contains reflection symmetry for the compounds (i.e., ABC is equivalent to CBA), we did not need to encode this

in the representation. Instead we sorted the bead arrangement when generating compounds for the importance sampling and machine learning.

V. SUPPORTING INFORMATION

The attached supporting information contains additional details on (i) the Monte Carlo sampling with the network structure; (ii) the optimization of thermodynamic cycles; (iii) the learning curves of the machine learning model; and (iv) results on linear tetramers. In addition, we provide databases for the transfer free energies of all trimers and tetramers, as well as atomistic-

resolution compounds that map to trimers in a repository [33].

ACKNOWLEDGMENTS

The authors thank Alessia Centi and Clemens Rauer for critical reading of the manuscript. The authors acknowledge Chemaxon for an academic research license of the Marvin Suite. This work was supported by the Emmy Noether program of the Deutsche Forschungsgemeinschaft (DFG) and the John von Neumann Institute for Computing (NIC) through access to the supercomputer JURECA at Jülich Supercomputing Centre (JSC).

-
- [1] E. O. Pyzer-Knapp, C. Suh, R. Gómez-Bombarelli, J. Aguilera-Iparraguirre, and A. Aspuru-Guzik, *Annual Review of Materials Research* **45**, 195 (2015).
- [2] A. Jain, Y. Shin, and K. A. Persson, *Nature Reviews Materials* **1**, 15004 (2016).
- [3] T. Bereau, D. Andrienko, and K. Kremer, *APL Materials* **4**, 6391 (2016).
- [4] O. A. von Lilienfeld, *Angewandte Chemie International Edition* **57**, 4164 (2018).
- [5] S. Curtarolo, G. L. Hart, M. B. Nardelli, N. Mingo, S. Sanvito, and O. Levy, *Nature materials* **12**, 191 (2013).
- [6] L. M. Ghiringhelli, J. Vybiral, S. V. Levchenko, C. Draxl, and M. Scheffler, *Physical review letters* **114**, 105503 (2015).
- [7] A. L. Ferguson, *Journal of Physics: Condensed Matter* **30**, 043002 (2017).
- [8] T. Bereau, “Data-driven methods in multiscale modeling of soft matter,” in *Handbook of Materials Modeling: Methods: Theory and Modeling*, edited by W. Andreoni and S. Yip (Springer, 2018) pp. 1–12.
- [9] W. G. Noid, *J. Chem. Phys.* **139**, 090901 (2013).
- [10] T. Bereau and K. Kremer, *J. Chem. Theory Comput.* **11**, 2783 (2015).
- [11] X. Periole and S.-J. Marrink, in *Biomolecular Simulations* (Springer, 2013) pp. 533–565.
- [12] R. Menichetti, K. H. Kanekal, K. Kremer, and T. Bereau, *The Journal of Chemical Physics* **147**, 125101 (2017).
- [13] R. Menichetti, K. H. Kanekal, and T. Bereau, *ACS Central Science* **5**, 290 (2019).
- [14] J. Mongan, D. A. Case, and J. A. McCammon, *Journal of computational chemistry* **25**, 2038 (2004).
- [15] C. E. Rasmussen, in *Advanced lectures on machine learning* (Springer, 2004) pp. 63–71.
- [16] T. Fink and J.-L. Reymond, *J. Chem. Inf. Model.* **47**, 342 (2007).
- [17] M. Rupp, A. Tkatchenko, K.-R. Müller, and O. A. Von Lilienfeld, *Physical review letters* **108**, 058301 (2012).
- [18] F. A. Faber, A. Lindmaa, O. A. Von Lilienfeld, and R. Armiento, *Physical review letters* **117**, 135502 (2016).
- [19] A. P. Bartók, S. De, C. Poelking, N. Bernstein, J. R. Kermode, G. Csányi, and M. Ceriotti, *Science advances* **3**, e1701816 (2017).
- [20] L. Zhang, J. Tan, D. Han, and H. Zhu, *Drug discovery today* **22**, 1680 (2017).
- [21] R. V. Swift and R. E. Amaro, *Chemical biology & drug design* **81**, 61 (2013).
- [22] R. Ramakrishnan, P. O. Dral, M. Rupp, and O. A. Von Lilienfeld, *Scientific data* **1**, 140022 (2014).
- [23] B. Sanchez-Lengeling and A. Aspuru-Guzik, *Science* **361**, 360 (2018).
- [24] F. A. Faber, L. Hutchison, B. Huang, J. Gilmer, S. S. Schoenholz, G. E. Dahl, O. Vinyals, S. Kearnes, P. F. Riley, and O. A. Von Lilienfeld, *Journal of chemical theory and computation* **13**, 5255 (2017).
- [25] G. Bussi, D. Donadio, and M. Parrinello, *J. Chem. Phys.* **126**, 014101 (2007).
- [26] M. Parrinello and A. Rahman, *J. Appl. Phys.* **52**, 7182 (1981).
- [27] T. A. Wassenaar, H. I. Ingólfsson, R. A. Böckmann, D. P. Tieleman, and S. J. Marrink, *J. Chem. Theory Comput.* **11**, 2144 (2015).
- [28] M. R. Shirts and J. D. Chodera, *J. Chem. Phys.* **129**, 124105 (2008).
- [29] P. V. Klimovich, M. R. Shirts, and D. L. Mobley, *Journal of computer-aided molecular design* **29**, 397 (2015).
- [30] K. Paton, *Communications of the ACM* **12**, 514 (1969).
- [31] M. Avriel, *Nonlinear programming: analysis and methods* (Courier Corporation, 2003).
- [32] F. A. Faber, A. S. Christensen, B. Huang, and O. A. von Lilienfeld, *The Journal of Chemical Physics* **148**, 241717 (2018).
- [33] C. Hoffmann, R. Menichetti, K. H. Kanekal, and T. Bereau, “Drug-membrane transfer free energies for coarse-grained trimers and tetramers,” <http://doi.org/10.5281/zenodo.2630488> (2019).